

AEGIS
A PROGRAM TO CALCULATE THE AVERAGE
BEHAVIOR OF ELECTROMAGNETIC SHOWERS

A. Van Ginneken

March 2, 1978

I. Introduction

The propagation of electromagnetic showers (EMS) in matter has been one of the earliest problems studied by means of Monte Carlo (MC) methods.¹ There also exist a variety of analytic approximations mainly to predict the longitudinal behavior of EMS.² In recent years a number of MC computer codes to study EMS have become available.³ These calculations generally follow the EMS in full analogue fashion down to some low energy cut-off of the participating particles. The computing time required to simulate EMS in this fashion is roughly proportional to the incident energy. For energies of interest at Fermilab (≈ 1000 GeV) computing times may become prohibitively long even on a fast computer.

For many applications a full analogue treatment is not necessary. This includes the important case of calculating average EMS energy deposited in matter as a function of location,

which is useful in studying, e.g. radiobiological dose, heating effects and radiation damage.

This note concerns a simple EMS program (AEGIS) which estimates average energy deposited as a function of position in a target of arbitrary (three dimensional) geometry and composed of any number of materials. Magnetic fields may be included in the calculation. AEGIS can be incorporated as a sub-program in CASIM^{4,5} to estimate energy deposition in hadron cascades due to EMS following π^0 decay. Previously CASIM used a simple algorithm based on a parametrization of various experimental and calculated results.

The motivation of the present work is (1) to have available a fast and reliable program to calculate high energy EMS, (2) the ability to include magnetic fields in EMS calculations and (3) to test the validity of the algorithm used in CASIM. As will be shown, results of the two methods are quite close. This validates a number of earlier results^{6,7} and lends added confidence to future use of the CASIM EMS algorithm (where computing speed is desired). In turn, the comparison may be viewed as a test of AEGIS versus data and calculated results upon which the algorithm is based (predominantly in the few GeV energy range). In addition, AEGIS results will be compared with recent high energy (100-300 GeV) data on EMS in lead-nuclear emulsion targets.⁸ Finally, the effects of a magnetic field on EMS will be illustrated by two examples. Some detail on the basic formulae and algorithms employed is collected in the Appendix.

II. Program AEGIS

The only particles considered in the calculation are electrons and photons. Their dominant interactions which govern the EMS behavior are well established.⁹ For electrons (and positrons) these include energy loss by ionization and excitation of the medium, multiple Coulomb scattering and bremsstrahlung. Photons are assumed to undergo Compton scattering and convert into electron pairs. Other interactions are neglected at the present level of desired accuracy.

AEGIS is specifically written for EMS with high initial energy. The approximate expressions of the differential cross sections used for bremsstrahlung and pair production (see Appendix) assume the energy of the incoming particle to be much larger than the electron rest energy. Nonetheless, AEGIS considers photons as low as 10^{-4} GeV because the Compton process dominates at sufficiently low energies and is accurately described by the Klein-Nishina cross-section formula. Pair production is neglected below 1.25 MeV and is described by the Bethe and Heitler incomplete screening formulae⁹ above this energy. When an electron is produced or is slowed down to below 5 MeV, its residual range is calculated and its energy is deposited in a randomly selected location along the produced trajectory. (For Compton electrons only the kinetic energy is deposited.) Since sub-5 MeV electrons lose almost all their energy by collision and since their range does not exceed a few g. cm^{-2} this approximation is justified. Collision losses of electrons are deposited locally at uniformly spaced steps along their trajectories. They are derived from a

stopping power vs. momentum table based on the formulae of Rohrlich and Carlson.¹⁰ Multiple Coulomb scattering of electrons is calculated at each step using a two component angular distribution: a Gaussian distribution (in projected angle) plus a single scattering tail (see Appendix). The particles emerging from a bremsstrahlung or pair production vertex assume the direction of the incident particle. This is justified at the level of a few percent of the typical opening angle of the EMS.¹¹ For the Compton process the directions of the outgoing particles are calculated using the Klein-Nishina formula. More details can be found in the Appendix.

The tracking of particles through a medium of arbitrary geometry and number of constituent materials is done in the same manner as in the program CASIM.^{4,5} Likewise, weighting techniques are applied similarly in both programs. Thus, each generation is represented by a single particle. This has advantages vis-a-vis analogue calculations in simplicity of coding, better efficiency and greater flexibility. A disadvantage is that correlations between particles are not included making the program generally unsuitable for use where correlations are important such as in so called "fluctuation problems".

Because of the approximate nature of the selection procedures energy is not conserved at each event vertex. Therefore, the total energy deposited by any particular (MC) EMS does not exactly equal the primary energy. Instead it is observed to follow a Gaussian distribution with a standard deviation (σ) of about

7% of the incident energy. The energy deposited summed over many primaries is slightly but systematically above the incident energy. This effect has been noticed at roughly the 2σ level (σ of the average) and is attributable to errors of interpolation. In a typical problem this is about 0.1% of the incident energy hence should be tolerable for most applications. The computer time required per incident particle varies logarithmically with primary energy and ranges from about 15 msec at 1 GeV to about 40 msec at 1000 GeV on an IBM 370/195.

III. Results and Comparisons

The program CASIM^{4,5} includes an algorithm which calculates the energy deposition by EMS in a thick target as a function of location. The algorithm is based on a parametrization of data (in the 0.1-10 GeV range) and of calculated results. Ref. 4 presents the basic scheme. A low energy correction (applicable for incident electrons below 6 GeV) is described in Ref. 5. The algorithm is fast and relatively simple. It has not been tested directly at Fermilab energies although energy deposition as calculated by CASIM (hadrons plus EMS) agrees well with results of two thick target experiments.^{6,7} However, such agreement is not too convincing of the validity of the EMS algorithm. In these experiments, hadron cascade development, finite beam size and finite detector size influence the spatial distribution of the energy deposition much more than does the EMS development.

Figures 1-3 present comparisons for an iron target between the CASIM algorithm and AEGIS. In Fig. 1 (a-d) the radially integrated depth dependence is shown for incident photons of energies 1-1000 GeV. The agreement is quite good particularly for the 1 GeV and 10 GeV cases which belong to the energy range where the algorithm has its basis. As the energy is increased the algorithm tends to predict a somewhat broader depth distribution. In Fig. 2 (a-d) the longitudinally integrated radial dependence is presented for photons of the same incident energies over the range 0-7 cm. The minimum radial bin was chosen to be 0.1 cm which is typical of beam dimensions. The results are expressed in GeV per cm (i.e. in a ring of unit width) for ease of radial integration. Agreement is quite satisfactory at all four energies. Above radii of 4 cm the algorithm predictions are consistently lower (typically by a factor of three at 6 cm radius). This confirms a tendency of the CASIM algorithm to underestimate data at large radii. This defect was noted when the algorithm was introduced in Ref. 4 but tolerated for simplicity. Fig. 3 (a-d) shows the maximum energy density as a function of radius for small radii (.0001-0.1 cm). Typically AEGIS predicts longer energy deposition by a factor of two with the larger discrepancies occurring at the smaller radii. Again this disagreement is not surprising since the radii explored here are much smaller than the beam dimensions employed in the experiments on which the algorithm is based. Figures 4-6 present the comparisons for a lead target in similar fashion. The situation is much like that for iron.

The comparisons shown here are quite a bit more extensive than need be to convey to most readers the degree of agreement between both calculations. However, it is hoped that the results being compared will be themselves useful as well as that they may serve to estimate the error incurred for calculations performed with the CASIM algorithm.

A recent Fermilab experiment⁸ measures the development of EMS showers in lead for 100 and 300 GeV electrons. The electrons are incident on a sandwich of lead plates (0.5 cm thick at 100 GeV; 0.25 cm thick at 300 GeV) and emulsion (0.005 cm thick, mounted on both sides of a 0.08 cm thick plastic backing). The total length of the stack is 5 cm at 100 GeV and 6 cm at 300 GeV. The experimenters report the depth dependence of tracks in the emulsion integrated from the beam axis out to four different radii (ranging from 0.00125 to 0.01 cm) as well as the radial distribution of track density at selected depths (over the 0.0005-0.01 cm range). Between 10 and 40 incident electrons are included in each sample. Both upstream and downstream emulsion layers are measured for the radial distribution. For the integrated depth dependence the upstream layer is counted at each location while the downstream layer is sampled less frequently. The experiment is considerably wider in scope but these are the only cases for which preliminary results are available.

To compare with AEGIS the program is modified to yield tracks in emulsion.¹² The geometry is simulated by a two

component medium: lead and a plastic-emulsion "amalgam". The (weighted) electrons crossing the front and back of the amalgam are separately tallied as a function of radius. These should provide good estimates of the data though slightly overestimating the front layer and slightly underestimating the back layer. The calculation ignores electrons below 5 MeV. An actual cut-off is not given in Ref. 8 but the results are not too sensitive to this assumption.

Figures 7 and 8 show the comparisons at 100 GeV for depth dependence and radial distribution respectively. It must be emphasized that these are absolute comparisons. The overall agreement is quite gratifying. The depth dependence shown in Fig. 7 (a-d) for the smaller radii exhibits a tendency to underestimate the data at the larger depths. This may be due to (a) poor statistics in the data, since the effect tends to disappear as the radius increases and (b) an experimental bias, revealed in Ref. 8, to identify the center of the shower at these deep layers with the highest track density. The calculation seems to fit the emulsion layers upstream of the plastic better than those downstream. The difference between the two appears larger in the calculation. This might be a consequence of the above mentioned approximation used to estimate tracks at these locations. The radial distributions of Fig. 8 (a-d) while reflecting (in sum) the discrepancies noted for the depth dependence are otherwise in remarkably good agreement. It is to be noted that the hatched areas in Fig. 8 mark the spread between upstream and downstream layers and do not indicate uncertainties of the calculation.

Figures 9 and 10 compare the 300 GeV results. Agreement is again quite good. The depth dependence of Fig. 9 (a-d) the downstream layer is now fitted somewhat better (in contrast to the 100 GeV results). There is here also a tendency to overestimate the difference between front and back layers though perhaps less marked than at 100 GeV. Likewise tracks at deep locations are overestimated by the calculation especially at small radii. Again the radial distributions of Fig. 10 (a-e) are in good agreement. A more meaningful comparison must await further analysis of the data. In Ref. 8 is shown a fit of the data to analytical calculations.¹³ No details of the parameters of this calculation are given though it may be presumed they were performed for a single medium. The fit is comparable to the one presented here. The greater versatility of the MC method for applications to multi-media, non-standard geometries, magnetic fields, etc. vis-a-vis analytical methods is worth pointing out here.

Figure 11 (a, b) illustrates how a uniform magnetic field of 40 kG influences EMS development. The graphs show the maximum energy deposited in iron by 1 GeV and 1000 GeV photons at small radii for two azimuthal regions (0 to 0.1 and 1 to $\pi/2$). Since photons are incident there is reflection symmetry both about the \vec{B} axis and the axis perpendicular to \vec{B} and the incident photon. As can be seen, the difference may amount to about a factor of three in energy deposition between the two regions. This may have significant consequences on the energy

deposited by beam losses in superconducting magnets. Figure 11 may be compared with Fig. 3 (a and d) although these were not run with correlated random numbers. Hence, there may be considerable statistical uncertainties in some regions.

My thanks to M. Awschalom, L. Coulson, H. Edwards and P. Gollon for their helpful comments.

APPENDIX

Production Cross Sections and Selection Procedures

The production cross sections assumed in the calculation are well known and widely available (e.g. Ref. 9). However, for convenience of the reader interested in programing considerations they are reproduced here along with the selection procedures derived from them.

In this problem there are always exactly two outgoing particles per event. Hence, selecting energy and direction of one particle determines the event completely. This leads to two alternate selection schemes: (a) choose the particle's energy, T , with a probability (roughly) proportional to the differential cross section, $d\sigma/dT$, and then decide whether to follow either this particle or its outgoing partner with a probability proportional to each particle's energy, (b) choose equally between the two outgoing particle types and use a selection function (roughly) proportional to $Td\sigma/dT$. Both schemes are used, as indicated below.¹⁴

Bremsstrahlung. The incomplete screening cross sections of Bethe and Heitler are assumed:

$$d\sigma/dv = Z(Z+1)\alpha r_e^2 v^{-1} \\ \times \{ (1+E^2/E_0^2) [\phi_1(\gamma) - 4\log Z/3] - (2E/3E_0) [\phi_2(\gamma) - 4\log Z/3] \} \quad (\gamma < 2) \quad (A1a)$$

$$= Z(Z+1)\alpha r_e^2 v^{-1} \\ \times 4(1+E^2/E_0^2 - 2E/3E_0) [\log(2E_0 E/mc^2 v) - 1/2 - c(\gamma)] \quad (\gamma > 2) \quad (A1b)$$

where Z is the atomic number, α the fine structure constant, r_e the classical electron radius, ν the radiated photon energy, mc^2 the electron rest energy, E_0 and E the incident and outgoing electron energies and $\gamma \equiv (100mc^2\nu/E_0EZ^{1/3})$. The functions $\phi_1(\gamma)$, $\phi_2(\gamma)$ and $c(\gamma)$ are taken from Ref. 9 and are represented in tabular form in the program. For $\gamma > 15$, $c(\gamma)$ vanishes and (A1b) then corresponds to the no screening case.

The selection function employed is

$$S(\nu) = N(E_0)\nu^{-1}[1-\nu/E_0-3\nu^2/4E_0^2]f(\gamma) \quad (\text{A2})$$

where $N(E_0)$ is a normalizing factor and $f(\gamma)$ is defined by

$$f(\gamma) = B-\gamma[B-\log(200/0.8Z^{1/3})+1/2]/0.8 \quad (\gamma \leq 0.8) \quad (\text{A3a})$$

$$= \log(2E_0E/mc^2\nu)-1/2 \quad (\gamma > 0.8) \quad (\text{A3b})$$

with $B = 5.75 - (\log Z)/3$. $S(\nu)$ is a rough approximation to $d\sigma/d\nu$.

The selection proceeds in four stages: (1) ν is selected from a distribution proportional to ν^{-1} , (2) a uniform random number is compared with the expression in square brackets in (A2) and if larger a new ν is chosen, (3) a uniform random number is compared with $f(\gamma)/f(0)$ and if larger a new ν is selected. Finally (4) a uniform random number r is generated to decide whether to follow the photon ($r \leq \nu/E_0$) or the electron. The particle is then assigned a weight

$$W_{\gamma,e} = S^{-1}(\nu) (d\sigma/d\nu) / T_{\gamma,e} \quad (A4)$$

where $T_{\gamma} = \nu/E_0$ and $T_e = 1 - T_{\gamma}$ are the probabilities to choose a photon and electron, respectively.

The total cross sections are evaluated by integrating (A1) over ν between the limits $\nu = 10^{-4}$ GeV and $(E_0 - mc^2)$. The interaction lengths are evaluated and stored for each of 71 logarithmically spaced incident energies E_i , which span the energy range of 10^{-4} - 10^3 GeV. The factor $N(E_0)$ of (A2) is stored similarly in tabular form.

Compton Scattering. The Klein-Nishina formula is assumed. The differential cross section with respect to the outgoing photon energy is

$$d\sigma/d\nu = \pi r_e^2 (mc^2)^2 \nu_0^2 \times [\nu/\nu_0 + (m^2 + 2m\nu_0)/\nu_0 + (\nu_0^2 - 2m\nu_0 - 2m^2)/\nu_0 \nu + m^2/\nu^2] \quad (A5)$$

where ν varies from $\nu_0 mc^2 / (mc^2 + 2\nu_0)$ to ν_0 , the incident photon energy. Each of the four terms in the square brackets (A5) is integrated between the above limits and their sum normalized to unity, for each incident energy E_i of the 71 member set referred to above. The results for the first three terms are stored in a table. The event selection proceeds by choosing a term from among the four terms of (A5) with probabilities proportional to the relative magnitudes of the integrals. Next a specific ν is

selected from a distribution proportional to that of the chosen term of (A5). Note that thus far the selection is unbiased. Finally the decision is made to follow the photon or electron in the same way as for bremsstrahlung. Here a weighting factor is assigned: $w_\gamma = \nu_0/\nu$ or $w_e = \nu_0/(\nu_0 - \nu)$.

The total cross sections corresponding to the integral of (A5) over ν are readily obtained in closed form. They are computed for each E_i and stored in an array.

Pair Production. Again the incomplete screening formulae are assumed:

$$d\sigma/dE_+ = Z(Z+1)\alpha r_e^2 \nu_0^{-3} \times \{(E_+^2 + E_-^2) [\phi_1(\gamma') - (4/3)\log Z] + (2/3)E_+E_- [\phi_2(\gamma') - (4/3)\log Z]\} \quad (\gamma' \leq 2) \quad (A6a)$$

$$= Z(Z+1) r_e^2 \nu_0^{-3} \times \{[E_+^2 + E_-^2 + (2/3)E_+E_-] [\log(2E_+E_-/mc^2\nu) - 1/2 - c(\gamma')]\} \quad (\gamma' > 2) \quad (A6b)$$

where $\gamma' \equiv 100\nu_0 mc^2 / (E_+ E_- Z^{1/3})$ and E_+ and E_- are the positron and electron energies which appear symmetrically in (A6).

The selection function used is

$$S(E) = M(\nu_0) [(4/3)E^3/\nu_0^3 + E/\nu_0 - (4/3)E^2/\nu_0^2] g(\gamma') \quad (A7)$$

with $M(\nu_0)$ a normalizing factor and $g(\gamma')$ defined as

$$g(\gamma') = B - \gamma' [B - \log(200/0.8 Z^{1/3}) + 1/2] / 0.8 \quad (\gamma' \leq 0.8) \quad (A8a)$$

$$= \log[2E(\nu_0 - E)/\nu_0 mc^2] - 1/2 \quad (\gamma' > 0.8) \quad (A8b)$$

Note that $S(E)$ is roughly proportional to $Ed\sigma/dv$. The selection again proceeds in stages: (1) E is selected uniformly between the kinematical limits, (2) a uniform random number is compared with the expression in square brackets in (A5) and if larger a new E is selected, and (3) a uniform random number is compared with $g(\gamma')/g(o)$ and if larger a new E is selected. The particle is taken to be an electron or positron with equal probability. The weight in either case is

$$w = 2S^{-1}(E)(d\sigma/dE) \quad (A9)$$

The total cross section is obtained by integrating (A6) over the kinematical limits. These are calculated and stored for each of the E_i . They are also combined with the Compton total cross sections to obtain the photon interaction lengths.

Multiple Coulomb Scattering. A rather simple straightforward procedure is employed assuming all energies are much larger than the electron rest energy. The angular distribution of the electrons traversing a thickness t is assumed to be composed of an exponential distribution in the variable θ^2 ($\theta \equiv$ space angle) plus a single (Rutherford) scattering tail for $\theta > \theta_0$ ($\equiv 0.0175t^{1/2}/pX_0^{1/2}$, where X_0 is the radiation length of the medium and p is the momentum in GeV/c). The exponential distribution in θ^2 is equivalent to a Gaussian distribution in projected angle. The mean square angle is assumed to be¹⁵

$\theta_m = \theta_o [1 + 0.125 \log_{10}(t/0.1X_o)]$. The total probability for single scattering $\theta > \theta_o$ as measured by the integral of the single scattering distribution (using the small angle approximation and ∞ as upper limit) is independent of thickness or momentum (it is of the order of 0.02). This simplifies the algorithm.

REFERENCES

1. R. R. Wilson, Phys. Rev. 86, 261 (1951).
2. Reviews of analytical methods may be found in B. Rossi, High-Energy Particles, Prentice-Hall, Englewood Cliffs, N.J. (1952) and J. Nishimura, Theory of Cascade Showers in Vol. XLIV/2 of Handbuch der Physik, S. Flügge, Ed., Springer Verlag, Berlin (1967).
3. For example: J. C. Butcher and H. Messel, Phys Rev. 112, 2096 (1958) and successive versions; C. D. Zerby and H. S. Moran, A Monte Carlo Calculation of the Three-Dimensional Development of High-Energy Electron-Photon Cascade Showers, ORNL-TM-422 (1962); R. L. Ford and W. R. Nelson, The EGS Code System. Program for Monte Carlo Simulation of Electromagnetic Cascade Showers, Version III, SLAC Report, (in preparation).
4. A. Van Ginneken and M. Awschalom, High Energy Particle Interactions in Large Targets, Vol. I, Fermilab, Batavia, IL (1974).
5. A. Van Ginneken, CASIM. Program to Simulate Hadronic Cascades in Bulk Matter, Fermilab, FN-272 (1975).
6. M. Awschalom et al., Nucl. Inst. Meth., 131, 235 (1975).
7. M. Awschalom et al., Nucl. Inst. Meth., 138, 521 (1976).
8. S. Dake et al., The Electromagnetic Cascade Showers in Lead Absorber, Kobe University preprint (1977).
9. See e.g. H. A. Bethe and J. Ashkin, Passage of Radiations Through Matter in Experimental Nuclear Physics, Vol. I, E. Segre, Ed., Wiley, N. Y. (1953).
10. F. Rohrlich and B. C. Carlson, Phys. Rev. 93, 38 (1954).
11. B. Rossi and K. Greisen, Rev. Mod. Phys. 13, 240 (1941).
12. The number of tracks can be simply identified with the weight assigned to electrons at each location. The basic MC scheme is identical to that for computing energy deposition. To ensure fast convergence of the calculation use of "recording particles" is made here. To estimate electron track density electron emission is simulated at each vertex with the electrons kinematical parameters selected from a distribution proportional to the differential cross section (rather than differential inelasticity). This is entirely similar to the use of recording particles in CASIM described in Ref. 7.

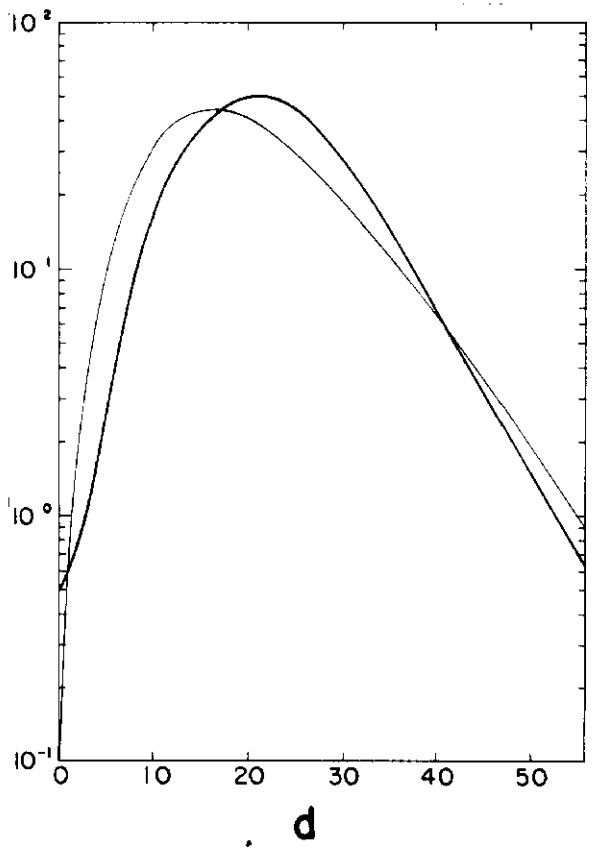
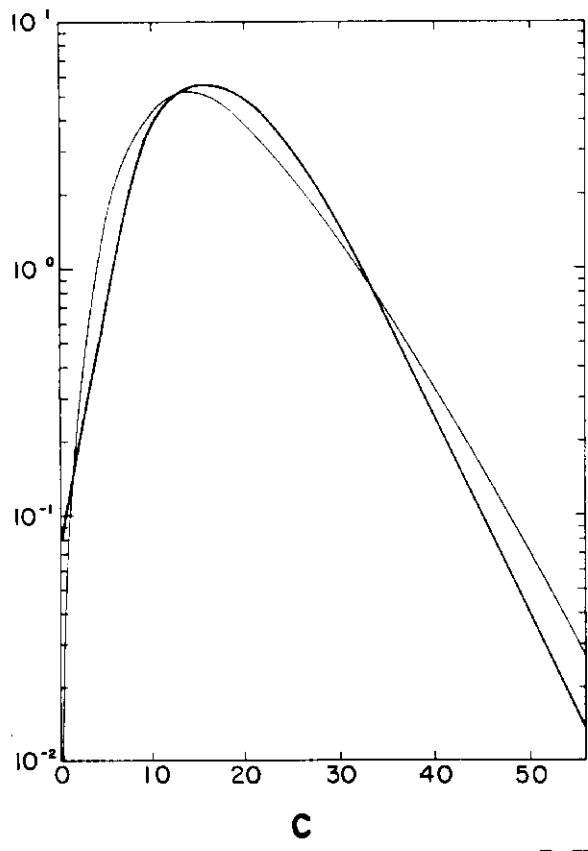
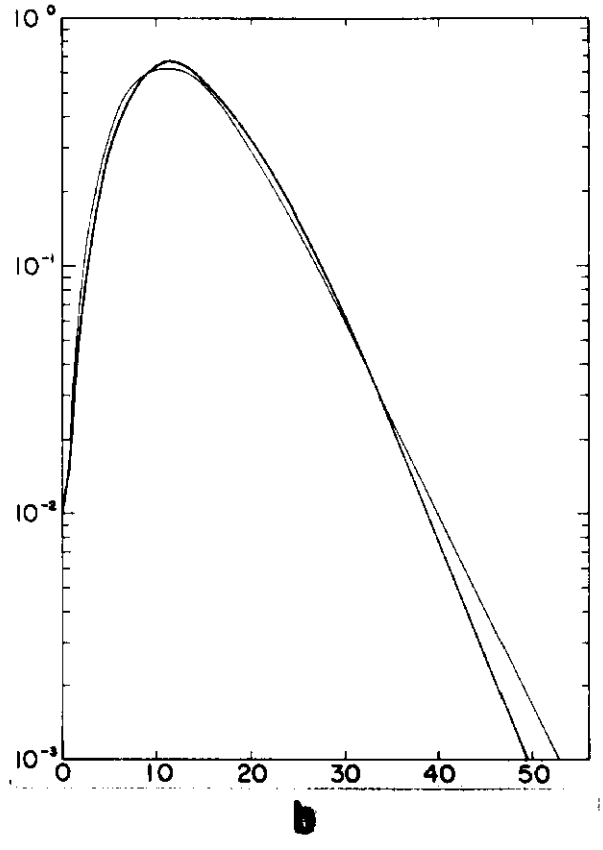
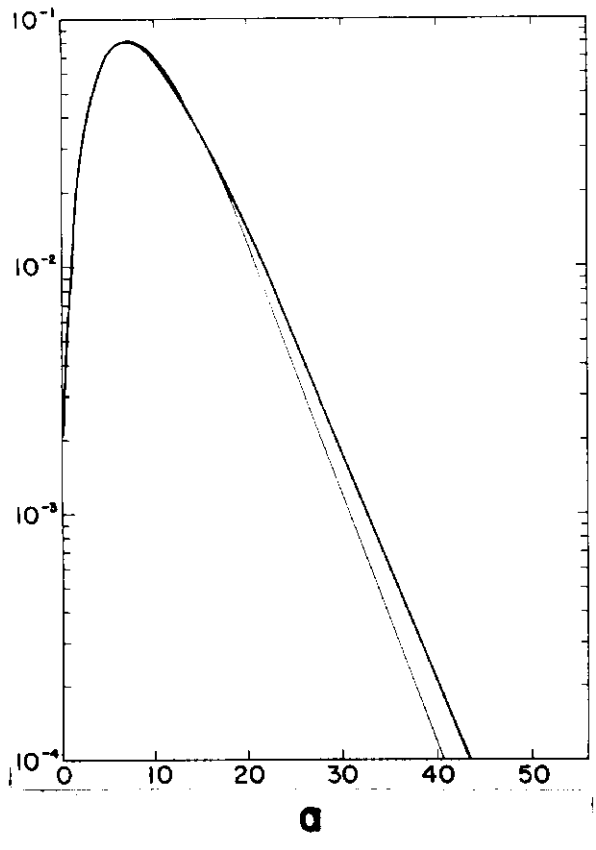
13. J. Kidd and J. Nishimura, Suppl. Nuovo Cim. 1, 1086 (1963).
14. This could be generalized to include any combination of the two selection functions with product equal to $Td\sigma/dT$. This has not been attempted here. In principle, this could be exploited e.g. to simplify coding or speed execution.
15. V. Highland, Nucl. Inst. Meth., 129, 497 (1975).

Figure Captions

1. Radially integrated energy density in iron as a function of depth for incident photons of 1 GeV (a), 10 GeV (b), 100 GeV (c) and 1000 GeV (d). Thin curve is prediction of CASIM algorithm, heavy curve of AEGIS.
2. Longitudinally integrated energy deposition in iron as a function of radius for incident photons of 1 GeV (a), 10 GeV (b), 100 GeV (c) and 1000 GeV (d). Thin histogram is prediction of CASIM algorithm, heavy histogram of AEGIS. Note that ordinate is expressed in units of inverse (radial) distance for ease of integration.
3. Maximum energy density in iron as a function of radius for incident photons of 1 GeV (a), 10 GeV (b), 100 GeV (c) and 1000 GeV (d). Thin histogram is prediction of CASIM algorithm, heavy histogram of AEGIS.
4. Radially integrated energy density in lead as a function of depth for incident photons of 1 GeV (a), 10 GeV (b), 100 GeV (c) and 1000 GeV (d). Thin curve is prediction of CASIM algorithm, heavy curve of AEGIS.
5. Longitudinally integrated energy density in lead as a function of depth for incident photons of 1 GeV (a), 10 GeV (b), 100 GeV (c) and 1000 GeV (d). Thin histogram is prediction of CASIM algorithm, heavy histogram of AEGIS. Note that ordinate is expressed in units of inverse (radial) distance for ease of integration.
6. Maximum energy density in lead as a function of radius for incident photons of 1 GeV (a), 10 GeV (b), 100 GeV (c) and 1000 GeV (d). Thin histogram is prediction of CASIM algorithm, heavy histogram of AEGIS.
7. Radially integrated track density in nuclear emulsion embedded in lead for 100 GeV incident electrons. Open circles correspond to data in emulsion layer upstream of 800 μm plastic backing, closed circles to downstream layer. Top and bottom curves are AEGIS predictions resp. for the upstream and downstream layers. The track density is integrated from zero radius to 12.5 μm (a), 25 μm (b), 50 μm (c) and 100 μm (d).

8. Track density in nuclear emulsion embedded in lead for 100 GeV incident electrons at depths of 1 cm (a), 2 cm (b), 3 cm (c) and 4 cm (d) as a function of radius. Open circles correspond to data in emulsion layer upstream of 800 μm plastic backing, closed circles to downstream layer. AEGIS predictions for upstream and downstream layers are shown separated by hatched area.
9. Radially integrated track density in nuclear emulsion embedded in lead for 300 GeV incident electrons. Open circles correspond to data in emulsion layer upstream of 800 μm plastic backing, closed circles to downstream layer. Top and bottom curves are AEGIS predictions resp. for the upstream and downstream layers. The track density is integrated from zero radius to 12.5 μm (a), 25 μm (b), 50 μm (c) and 100 μm (d).
10. Track density in nuclear emulsion embedded in lead for 300 GeV incident electrons at depths of 0.75 cm (a), 1.75 cm (b), 2.75 cm (c), 3.75 cm (d), 4.75 cm (e) and 5.75 cm (f) as a function of radius. Open circles correspond to data in emulsion layer upstream of 800 μm plastic backing, closed circles to downstream layer. AEGIS predictions are shown separated by hatched area.
11. Effect of a uniform magnetic field of 40 kG on radial development of electromagnetic showers. The maximum energy deposition is shown as a function of radius for the azimuthal region 0-0.1 rad (heavy line) and 1- $\pi/2$ rad (thin line) for 1 GeV (a) and 1000 GeV (b) incident photons. The azimuthal angle is measured from axis perpendicular to both the incident photons and the magnetic field.

ENERGY DEPOSITED, $\text{GEV}\cdot\text{cm}^{-1}\cdot(\text{INC.}\gamma)^{-1}$



DEPTH, cm

FIG. 1

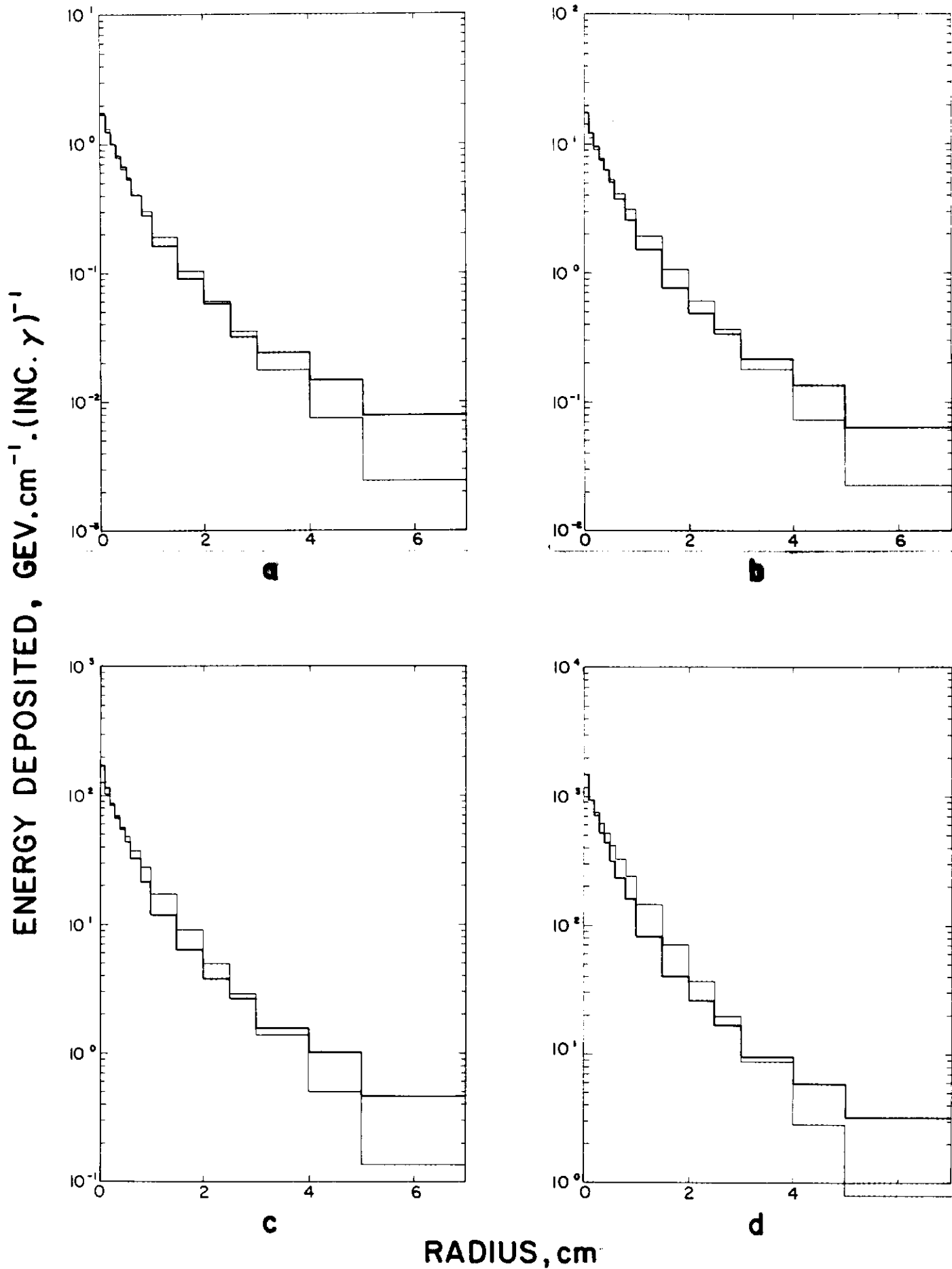


FIG. 2

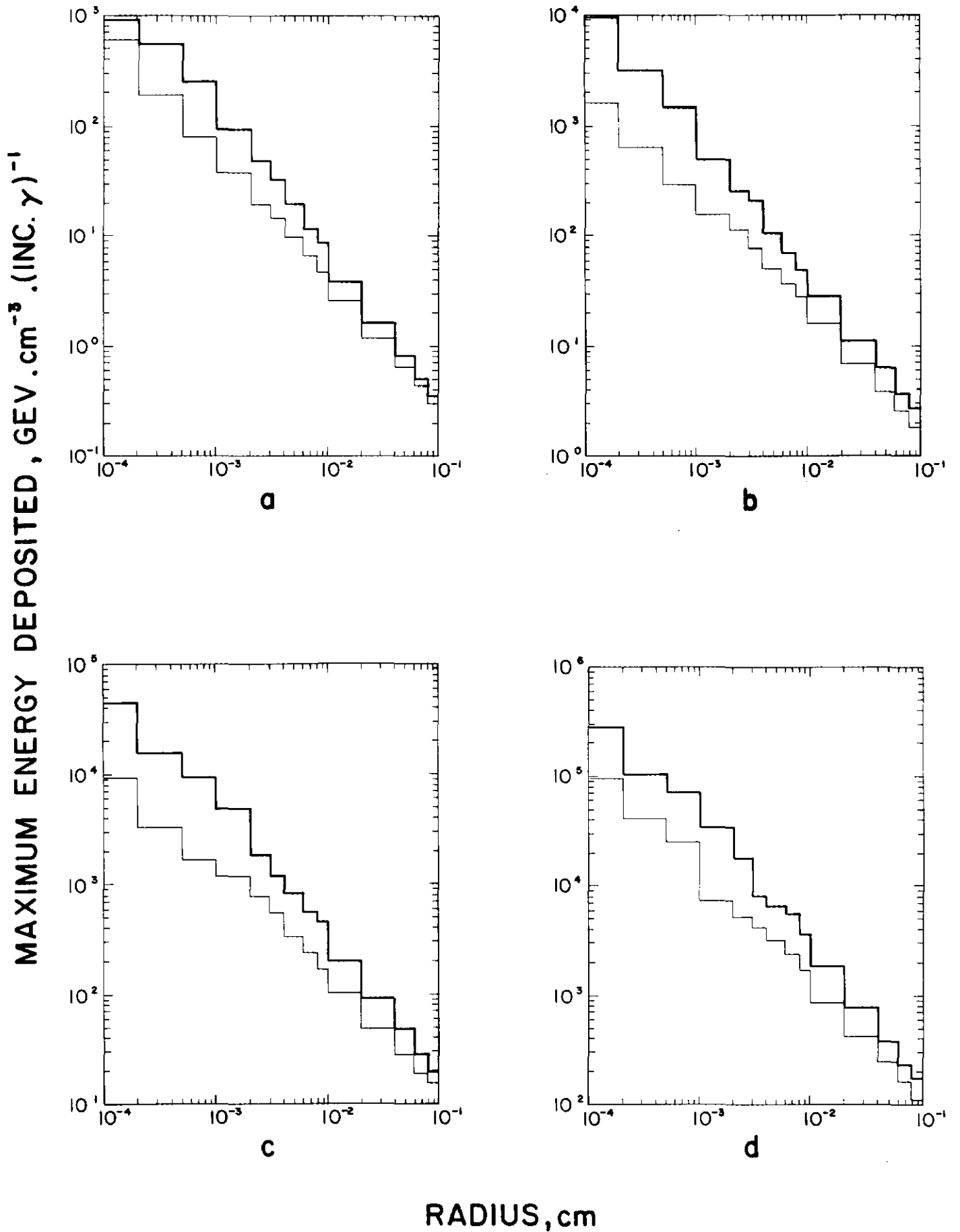


FIG. 3

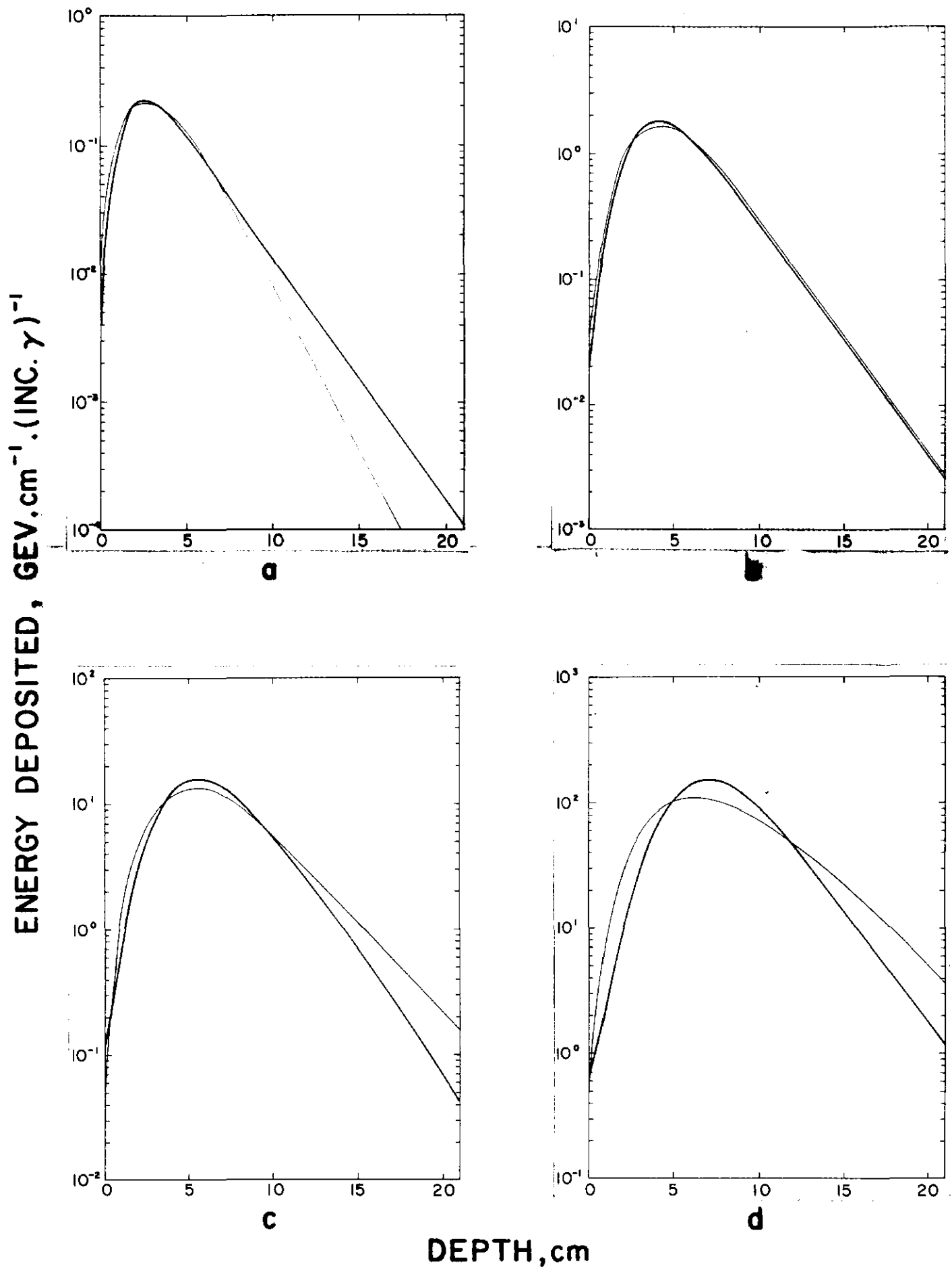
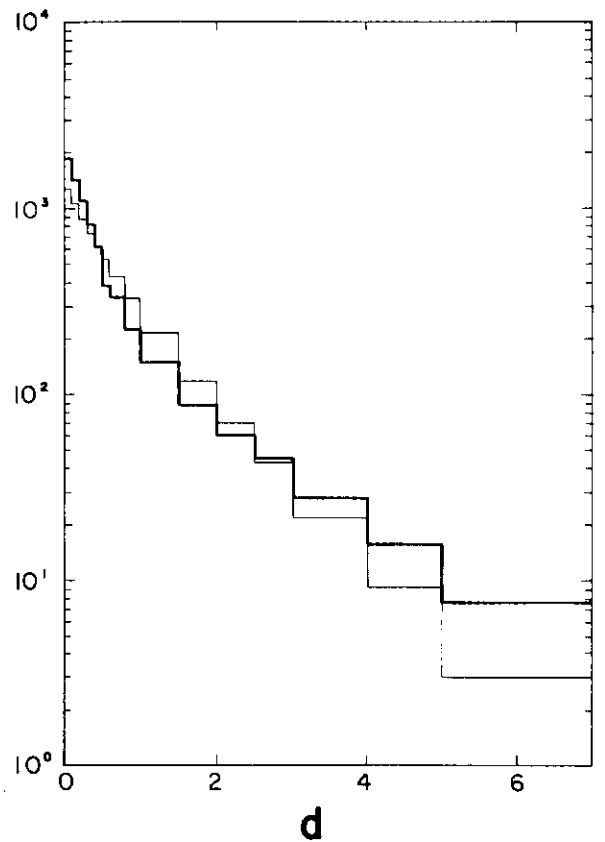
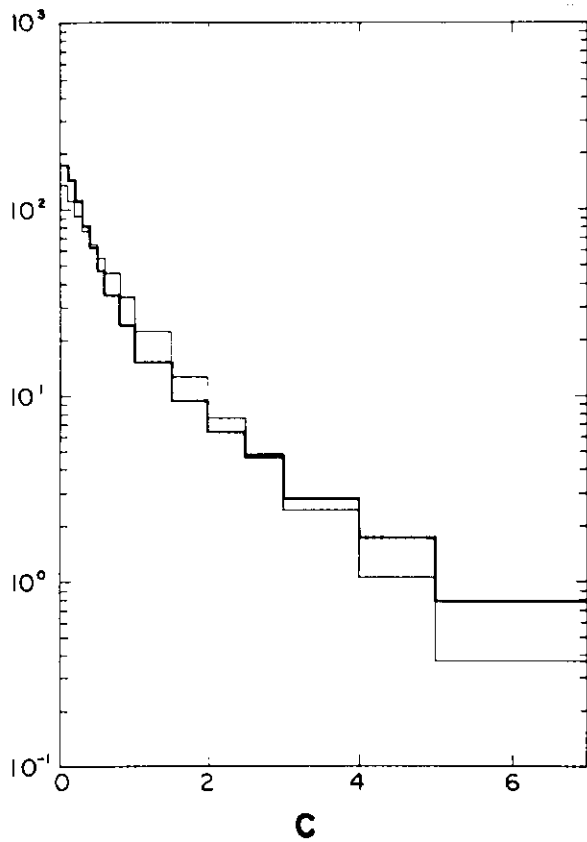
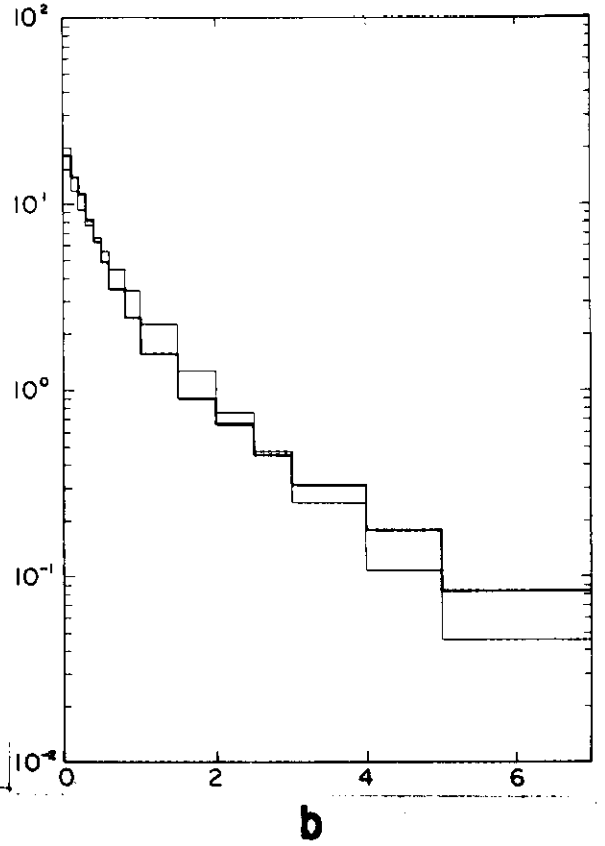
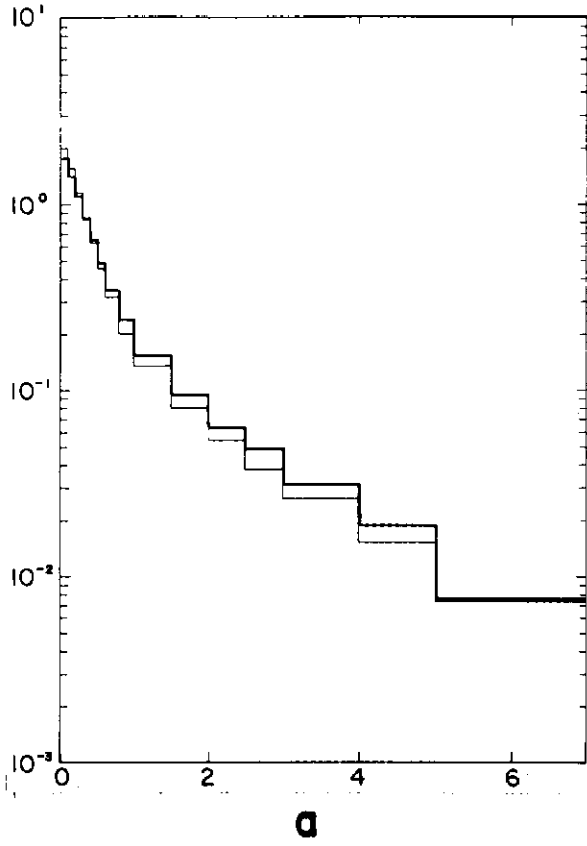


FIG. 4

ENERGY DEPOSITED, $\text{GEV}\cdot\text{cm}^{-1}\cdot(\text{INC.}\gamma)^{-1}$



RADIUS, cm

FIG. 5

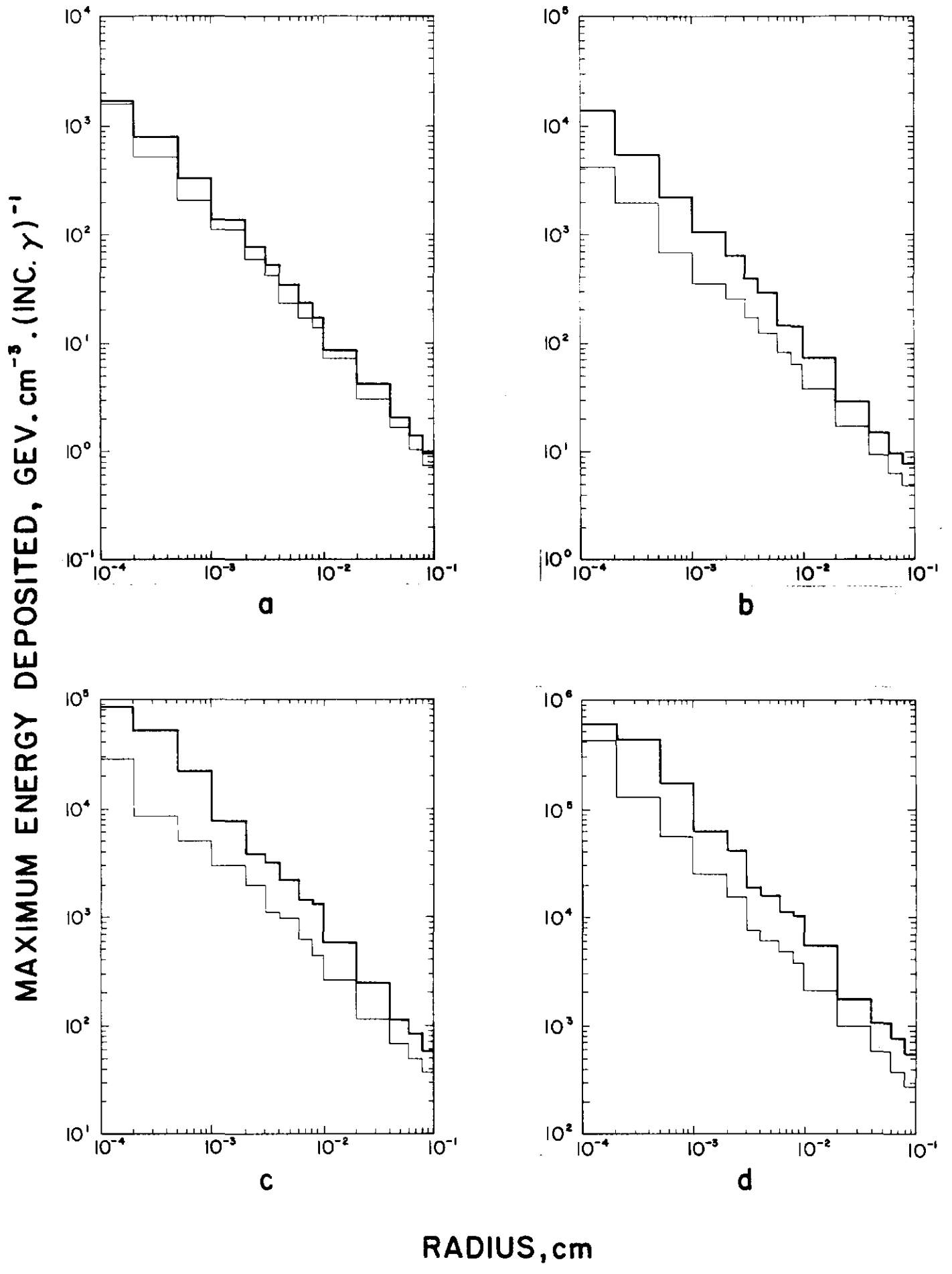
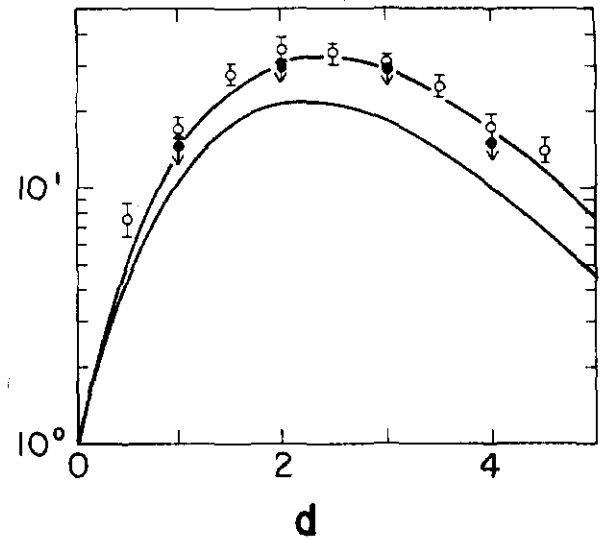
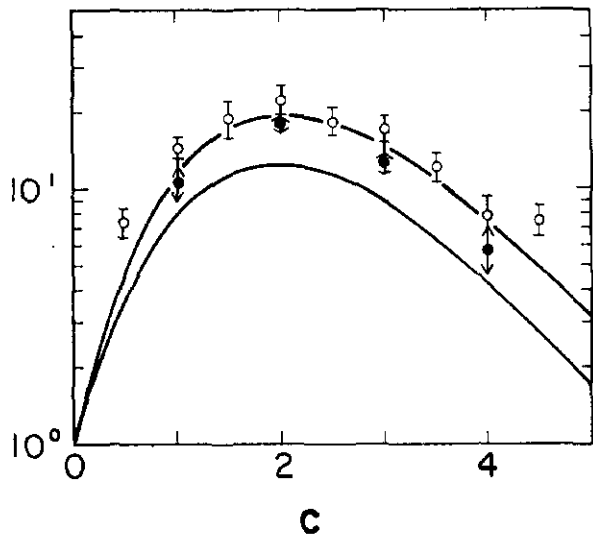
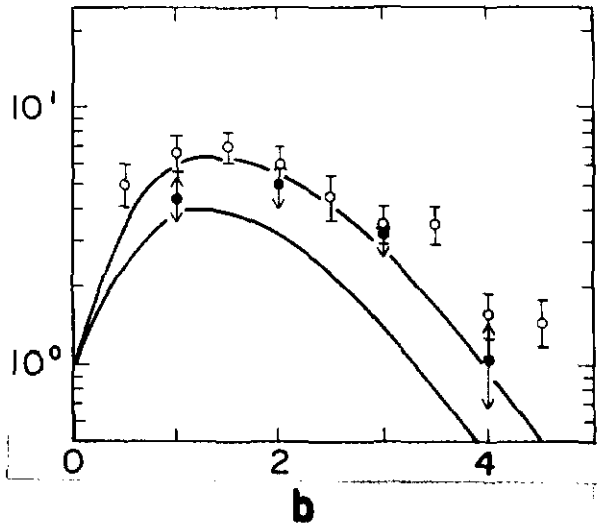
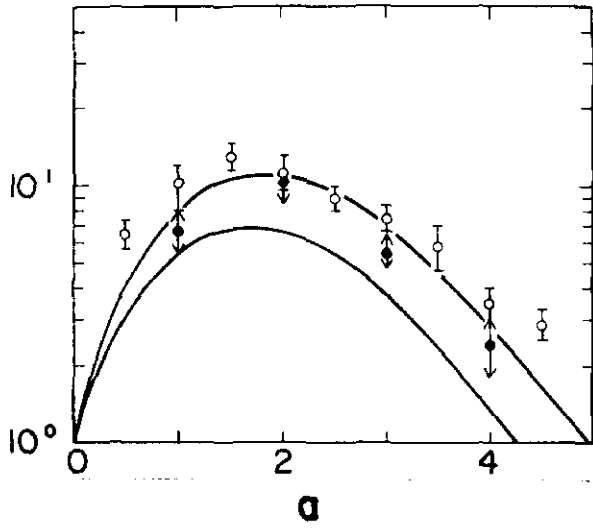


FIG. 6

TRACKS. (INC. e^-) $^{-1}$



DEPTH, cm OF LEAD

FIG. 7

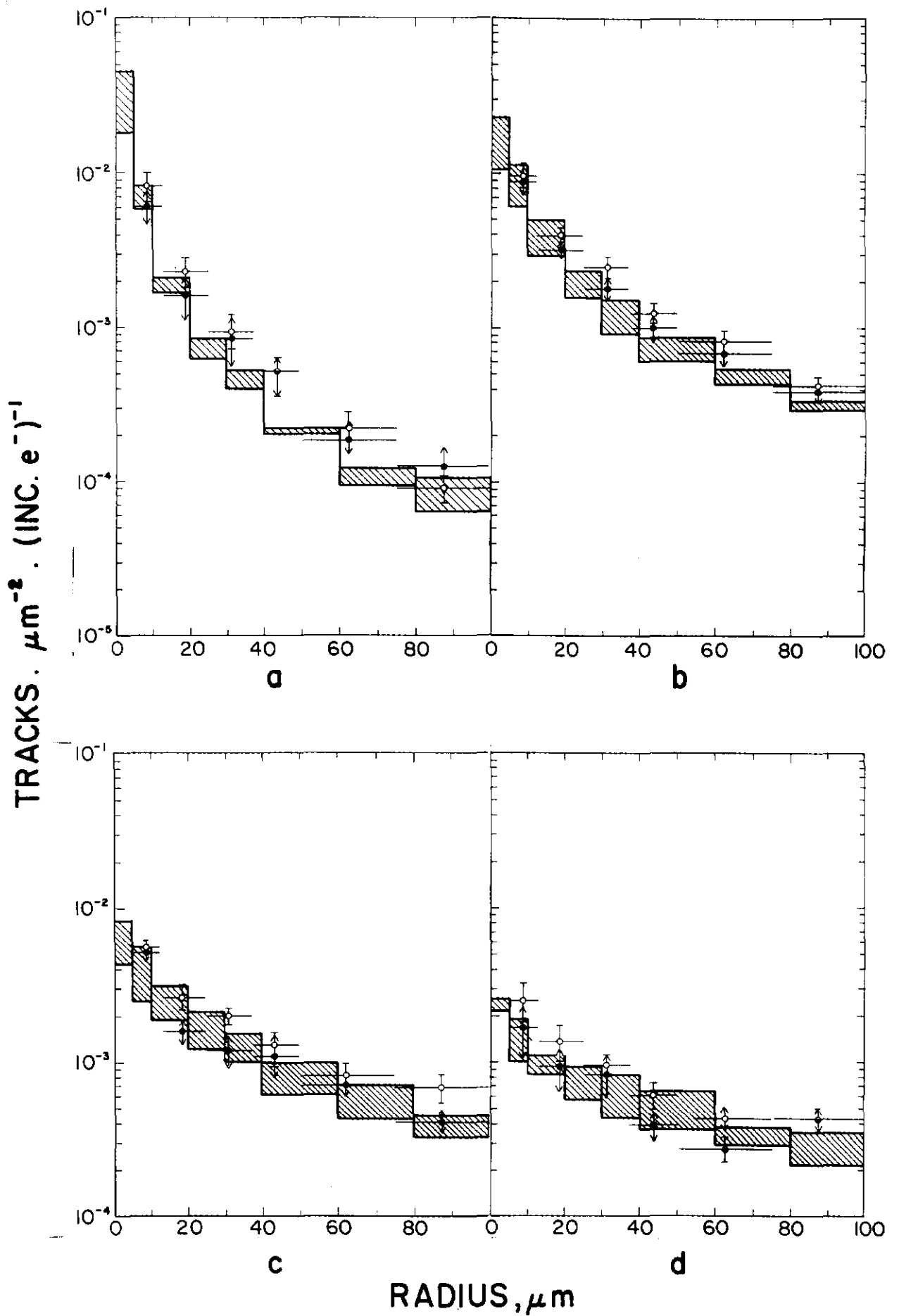


FIG. 8

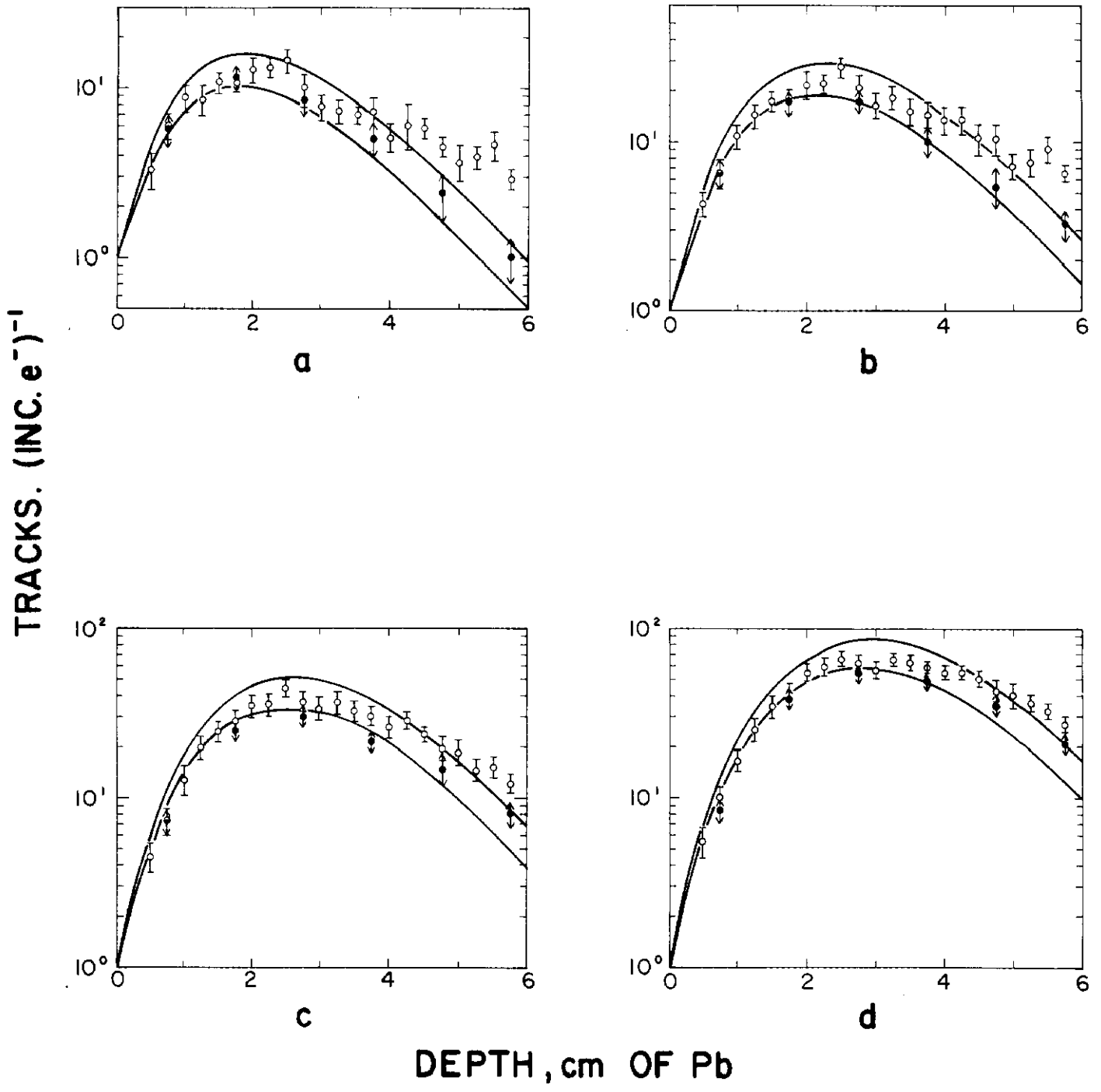


FIG. 9

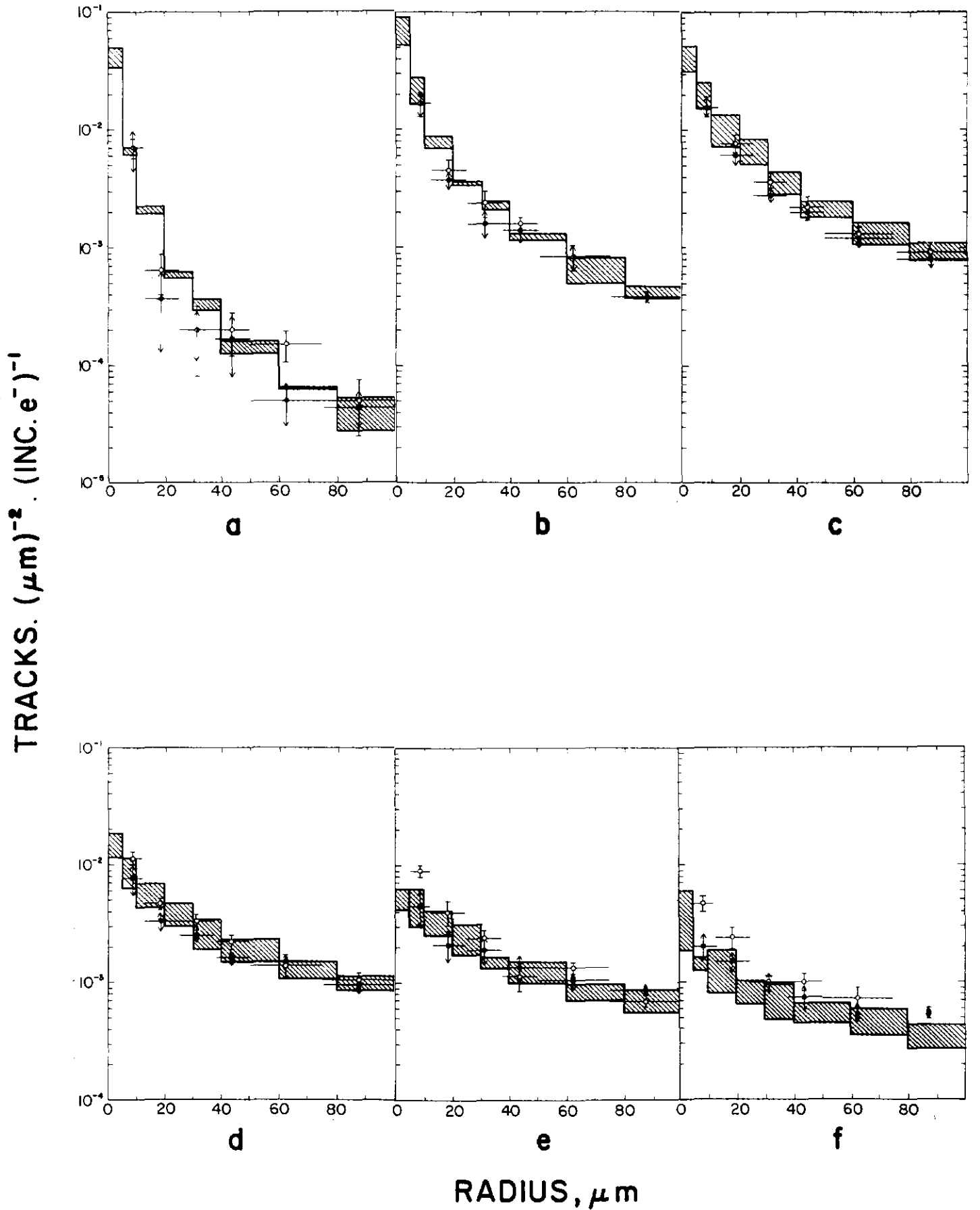
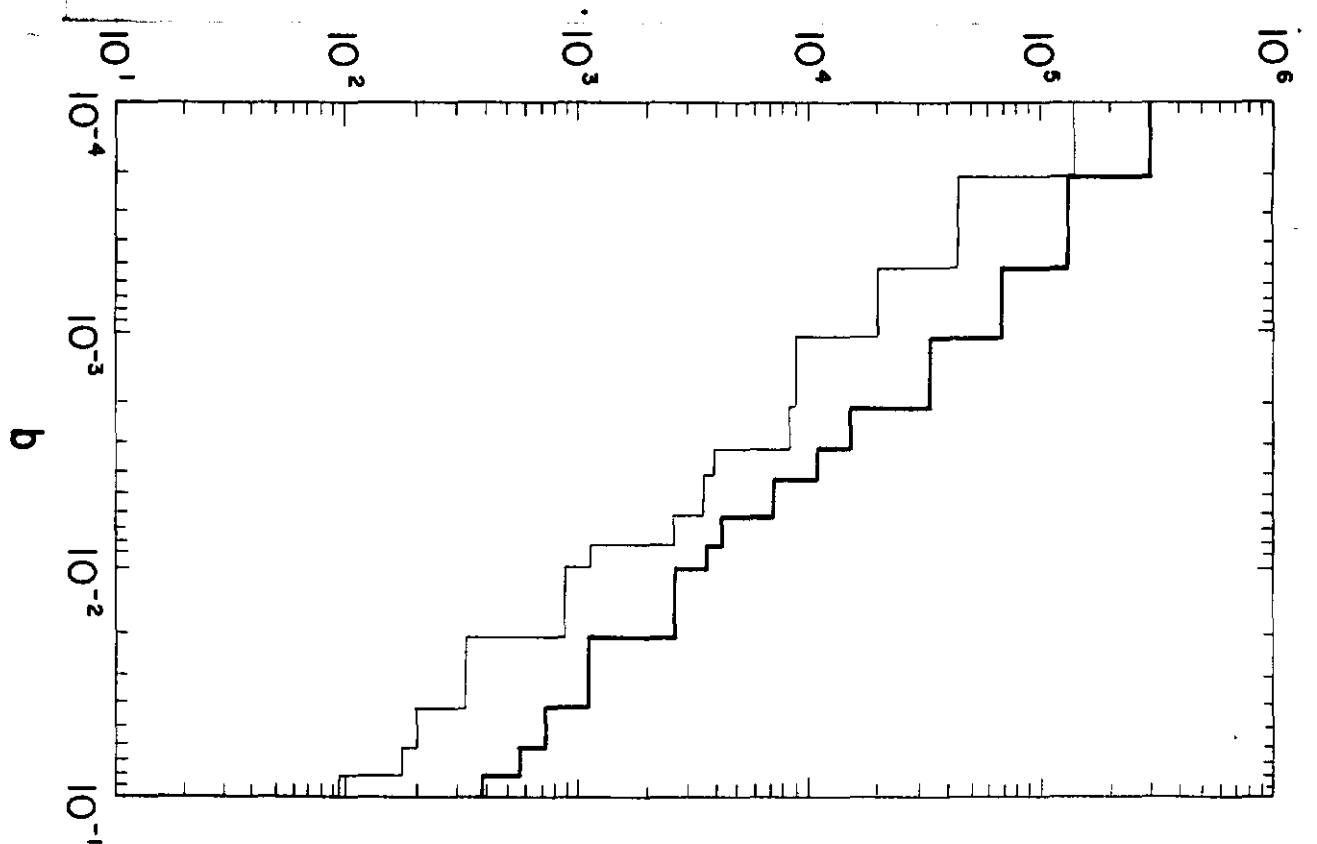
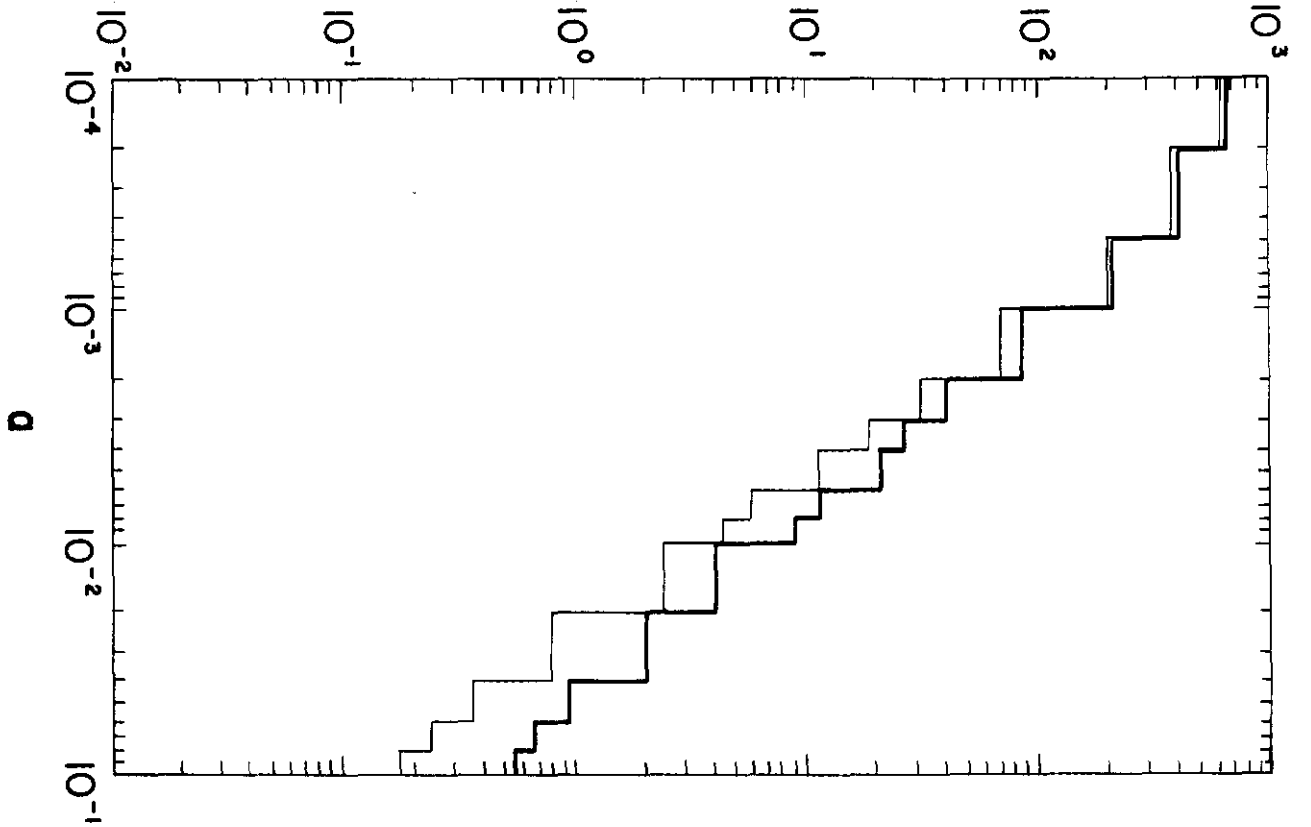


FIG. 10

MAXIMUM ENERGY DEPOSITED, $\text{GEV} \cdot \text{cm}^{-3} \cdot (\text{INC. } \gamma)^{-1}$



RADIUS, cm

FIG. 11